Performance Analysis of a Thermionic Thermal Detector at 400K, 300K, and 200K*

James E. Murguia*[a], Prabha K. Tedrow[a], Freeman D. Shepherd[a], Darin Leahy[b], and Melanie M. Weeks[b]

[a]Solid State Scientific Corporation 27-2 Wright Road Hollis NH 03049

[b]AFRL/SNHI Hanscom AFB, Bedford MA 01731

ABSTRACT

The Thermionic Thermal Detector (TTD) senses infrared radiation by temperature modulation of thermionic emission current within a silicon Schottky diode. The thermionic emission current is the well known Richardson dark current. The TTD operates in the LWIR band. The physics of TTD operation is distinct from that of silicon Schottky barrier MWIR detectors, such as PtSi/Si which are based on internal photoemission. In fact, the TTD has high detection efficiency. The architecture of a TTD array is very similar to that of microbolometer arrays, except the detector elements are thermally isolated Schottky diodes, operating under reverse bias. When the TTD array is illuminated by an infrared image, the temperature of individual detector elements will vary with the local incident power of the image. Under small signal conditions, the dark current of individual detectors will vary as temperature, resulting in an electronic image of the infrared scene.

The reverse bias dark current of a Schottky diode varies exponentially with temperature. For the small temperature variations observed on the focal plane of an uncooled sensor, this variation is approximately linear. The rate of temperature variation is determined by the Schottky barrier potential and, to a lesser extent by the applied bias potential. The operating temperature range of the detector can be designed into the device by selecting a metal with the appropriate Schottky barrier height. Experimental Schottky barrier heights were determined using Richardson dark current activation energy analysis. Devices optimized for operation at room ambient temperature have a 6%/K temperature coefficient. The use of Schottky diode thermionic emission for uncooled infrared imaging offers several advantages relative to current technology. TTD manufacture is 100% silicon processing compatible. Schottky barrier based thermionic emission arrays have the same uniformity characteristics as MWIR Schottky barrier photoemissive arrays. Operating TTDs in reverse bias provides a high impedance "current source" to the multiplexer, resulting in negligible Johnson noise. This mode of operation also results in negligible detector 1/f-noise and drift. In addition, the TTD thermionic emission detection process has high efficiency, fully comparable with the best current thermal detectors.

This paper describes the theoretical performance of a TTD based LWIR sensor. The focal plane architecture and multiplexer is similar to current microbolometer arrays, except the VO_x resistor is replaced with a TTD thermionic emission sensing element. The analysis models the detector using the appropriate optical radiation, thermal diffusion, and electrical conduction equations for 400K, 300K and 200K operation, using three different metal silicides. The effects of the optical radiation noise, thermal diffusion noise, Johnson noise, shot noise, and amplifier noise are considered in the analysis. Samples of the TTD designed for operation at 300 K and suitable for integration with a multiplexer, were fabricated and electrically tested. The predicted NEDT for an uncooled LWIR sensor based on a TTD thermal sensing element is 6 mK

Keywords: thermal imaging, uncooled detection, Schottky diode thermionic emission, metal-silicide arrays.

1. INTRODUCTION

Under the sponsorship of the Defense Advanced Research Agency (DARPA), the Air Force Research Laboratory, Sensors Directorate (AFRL) and Solid State Scientific Corporation (SSSC) have developed the theory of operation for a silicon Schottky barrier based Thermionic Thermal Detector (TTD) for uncooled sensing of 8 to 14 μm, LWIR, radiation. In

* This work was supported by the Defense Advanced Research Projects Agency and the Air Force Research Laboratory Sensors Directorate

addition, we have fabricated sample detectors having electrical characteristics which would support a TTD based thermal imaging sensor with a 6 mK NEDT, based on the use of a current art read out multiplexer chip.

A TTD array employs metal-silicide/silicon Schottky diodes as thermal detectors. The individual Schottky detectors are thermally isolated, similar to current microbolometer technology. The Schottky diodes are operated under reverse bias, to achieve very high impedance and to minimize 1/f-noise. Under these conditions, the diode is dominated by thermionic emission dark current, which varies exponentially with the absolute temperature. For a fixed bias voltage and Schottky barrier height, the magnitude of the reverse bias current gives a direct measure of the absolute temperature of the diode.

Figure 1 is a schematic representation of a TTD focal plane array. The architecture is very similar to that of a VO_x based microbolometer array. The Schottky barrier thermal detector is suspended on a thermally isolated plate as shown in the figure. The diode current flow is perpendicular to the plate. The plate is heated, for a video frame time, by the local incident power of the image. The detector is electrically isolated and at zero bias. For a short read-out interval the detector is back biased and temperature sampled by measurement of its dark current. This current is compared to the dark current of a reference detector that is not exposed to the LWIR radiation. The difference in the currents is the signal. The diode dark current changes approximately 6% for every 1 C change in the temperature of the plate. In an f/1 camera system, the radiation from a 1K differential source at 300K, will raise the temperature of the detector plate by 10-20 mK, resulting in 0.1% change in the diode dark current. The sample current must be large enough to produce the required sensitivity, when scaled by the temperature coefficient and temperature rise of the plate. The sample current levels and noise performance of current art microbolometer multiplexer circuits will meet TTD sensor requirements.

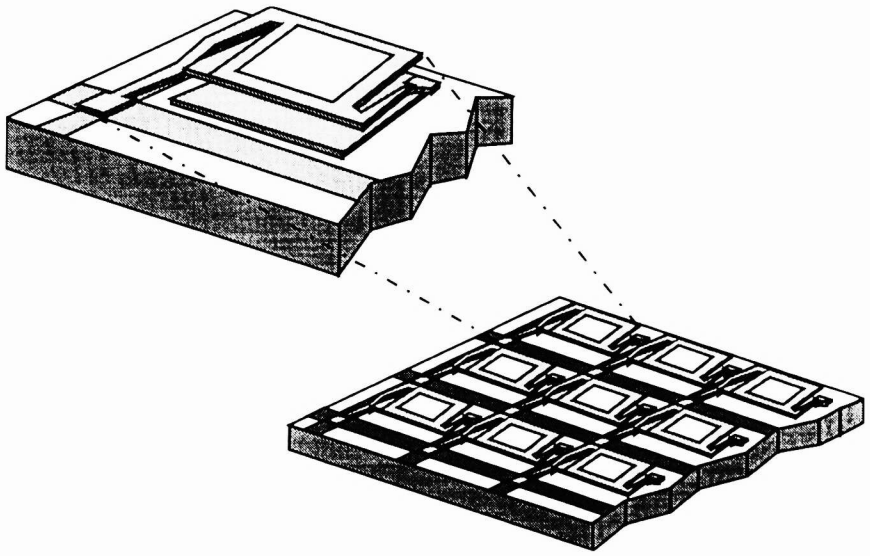

Figure 1: VO_x resistor based microbolometer, suspended on a thermally isolating membrane.

Relative to VO_x based microbolometer arrays, TTD arrays offer improved elemental temperature sensitivity, reduced noise, greater uniformity and better compatibility with silicon integrated circuit manufacturing.

Central to the development of the thermionic thermal detector is the maturation of three key microelectronic technologies; the fabrication of high ideality metal-silicide Schottky diodes with several barrier heights,[1] the micromachining of thermally isolated silicon microstructure arrays,[2,3,4] and the availability of high quality SIMOX and BESOI wafers.[5]

The subsequent sections describe the operation of the TTD in terms of the fundamental equations that govern its operation. Tables 1-2 define parameters used in the following development. Sections two through four provide a detailed description of the applicable optical, thermal and electrical equations that govern the operation of the TTD device element. Section five illustrates the affect of the multiplexer on the array. Section six defines the noise equivalent temperature (NEDT) of the array in terms of the equations derived in the previous sections. Finally, performance estimates for a TTD based thermal imaging system in low, ambient and high temperature operation are described in Section 7.

q	=	1.602×10^{-19} C	Charge on an electron.
A^{**}	=	30 $A \cdot cm^{-2} \cdot K^{-2}$	Richardson's Constant (p-type Si)
k	=	1.383×10^{-23} $J \cdot K^{-1}$	Boltzmann's constant.
ε_{Si}	=	1.054×10^{-12} $F \cdot cm^{-1}$	Dielectric constant of Si.
ε_{ox}	=	3.45×10^{-13} $F \cdot cm^{-2}$	Dielectric constant of thermal SiO_2.
π	=	3.14159	Value of Pi.
σ	=	5.67×10^{-12} $W \cdot cm^{-2} \cdot K^{-4}$	Stefan-Boltzmann constant.
h	=	6.625×10^{-34} J·sec	Planck constant

Table 1: Constants used in TTD analysis.

G_{Diff}		$W \cdot K^{-1}$	Thermal Diffusive Conductance.
G_{Rad}	$W \cdot K^{-1}$		Thermal Radiative Conductance.
G_{Therm}	$W \cdot K^{-1}$		Total Thermal Conductance.
κ	$W \cdot cm^{2} \cdot K^{-1}$		Thermal conductivity
C_{Therm}	$J \cdot K^{-1}$		Thermal heat capacitance of pixel.
Q_{Rad}	W		Heat radiated from detector.
Q_B	W		Heat radiated from background.
Q_S	W		Heat radiated from signal.
Q_{Bias}	W		Heat generated from bias.
Q_{Diff}	W		Heat transferred by diffusion.
P_S	W		Power radiated from signal.
P_B	W		Power radiated from background.
P_{Rad}	W		Power radiated from detector.
P_D	W		Power radiated on detector.
P_{DS}	W		Power radiated on detector from signal.
P_{DB}	W		Power radiated on detector from background.
T_S	K		Temperature of scene
T_B	K		Temperature of background
T_D	K		Temperature of detector
F			F number of system.
ε_D			Emissivity of Detector
ε_S			Emissivity of Target
ε_B			Emissivity of Background
V	V		Applied Bias Voltage on Schottky Diode.
qV_{bi}	J		Built in potential of Schottky Diode
N_D	cm^{-3}		Impurity concentration of p-type dopants
N_C	cm^{-3}		Density of states in Si conduction band.
Φ_{BO}	eV		Schottky barrier potential at zero bias
A_{Eff}	cm^{-2}		Detector effective active area
R_{Det}	Ω		Electrical resistance of detector (large signal)
R_{det}	Ω		Electrical resistance of detector (small signal)
R_F	Ω		Feedback resistance of amplifier
R_L	Ω		Load resistance on amplifier
Frame	s^{-1}		Frame rate.
S			Number of stages or pixels/column.
v_{na}	V		Input referred voltage noise of amplifier.
ρ	$g \cdot cm^{-3}$		Mass density
B	sec^{-1}		Bandwidth
c_s	$J \cdot K^{-1} \cdot g^{-1}$		Specific heat

Table 2: Variables used in TTD analysis.

2. OPTICAL RADIATION EQUATIONS

The heat flow from the surface of the detector via radiation follows the Stefan-Boltzmann law,

$$P_{Rad} = A_{Eff}\varepsilon_D\sigma T_D^4. \tag{2.1}$$

The thermal conductance of the detector due to radiation, G_{Rad}, is given by:[6]

$$G_{Rad} = 4A_{Eff}\varepsilon_D\sigma T_D^3 \tag{2.2}$$

In Equation 2.2, the detector pixel is approximated by a thin flat plate, which radiates in the forward direction and is assumed to be Lambertian. The optical power on a detector is the sum of the signal power and the background power,

$$P_D = P_{DS} + P_{DB} = \frac{A_{Eff}\varepsilon_D\sigma T_S^4}{4F^2+1} + \left(1 - \frac{1}{4F^2+1}\right)A_{Eff}\varepsilon_D\sigma T_B^4 \tag{2.3}$$

Equation 2.3 assumes the signal comes from an extended source at temperature T_S and the background radiation from the sensor enclosure at temperature T_B.

The emissivity of the background and the source is assumed to be one. Differentiating Equation 2.3, the change in power on a detector for an incremental change in signal temperature is given by,

$$\frac{dP_D}{dT_S} = \frac{dP_{DS}}{dT_S} = \frac{4A_{Eff}\varepsilon_D\sigma T_S^3}{4F^2+1}. \tag{2.4}$$

The radiation noise in a TTD with a thermal bandwidth of B is given by the noise equivalent power (NEP) due to radiation noise [1]

$$< NEP_{Rad} >^2 = 4kT^2BG_{Rad}. \tag{2.5}$$

3. THERMAL DIFFUSION EQUATIONS

The heat flow equation for the detector at temperature, T_D, is given by,

$$\rho c_s\frac{\partial T_D}{\partial t} = \kappa\left(\frac{\partial^2 T_D}{\partial x^2} + \frac{\partial^2 T_D}{\partial y^2} + \frac{\partial^2 T_D}{\partial z^2}\right) - Q_{Rad}^{out} + Q_B^{in} + Q_S^{in} + Q_{Bias}^{in} - Q_{Diff}^{out} \tag{3.1}$$

where, κ is the thermal conductivity of the Schottky diode, ρ is the mass density, c_s is the specific heat, and Q is the heat flow due to pixel radiation, incident enclosure radiation, incident radiation from the observed scene, diode bias, and thermal diffusion, respectively. A uniformly illuminated square pixel with a high thermal conductivity has a spatially uniform temperature distribution that can be approximated by,

$$\rho c_s\frac{\partial \Delta T_D}{\partial t} = -Q_{Rad}^{out} + Q_B^{in} + Q_S^{in} + Q_{Bias}^{in} - Q_{Diff}^{out}, \tag{3.2}$$

where ΔT_D is the temperature difference between the substrate chip and the detector pixel. In steady state, $\partial\Delta T_D/\partial t = 0$, and the power emitted from the detector is equal to the power incident onto the detector,

$$Q_{Rad}^{out} + Q_{Diff}^{out} = Q_B^{in} + Q_S^{in} + Q_{Bias}^{in} = P_{DS} + P_{DB} + Q_{Bias}^{in}. \quad 3.3$$

For a detector of area A_{Eff}, Equation 3.3 can be expressed as,

$$A_{Eff}\varepsilon_D\sigma T_D^4 + G_{Diff}(T_D - T_B) = \frac{A_{Eff}\varepsilon_D\sigma T_S^4}{4F^2+1} + \left(1 - \frac{1}{4F^2+1}\right)A_{Eff}\varepsilon_D\sigma T_B^4 + VI_{bias} \quad 3.4$$

where the terms correspond to the power radiated by the detector, the power thermally diffused from the detector, the power incident from the small signal onto the detector, the power incident from the enclosure onto the detector, and the power dissipated by the bias current, respectively.

The power on the detector, radiated from a small signal above background is adapted from Equation 2.3,

$$\delta P_{DS} = \frac{A_{Eff}\varepsilon_D\sigma T_S^4}{4F^2+1} \quad 3.5$$

Consequently:

$$A_{Eff}\varepsilon_D\sigma T_D^4 + G_{Diff}(T_D - T_B) = \delta P_{DS} + \left(1 - \frac{1}{4F^2+1}\right)A_{Eff}\varepsilon_D\sigma T_B^4 + VI_{bias} \quad 3.6$$

Rearranging terms,

$$A_{Eff}\varepsilon_D\sigma T_D^4 + G_{Diff}(T_D - T_B) - \left(1 - \frac{1}{4F^2+1}\right)A_{Eff}\varepsilon_D\sigma T_B^4 = \delta P_{DS} + VI_{bias}. \quad 3.7$$

Applying the operator $\partial/\partial T_D$ on both sides of the equation and substituting G_{Rad} of Equation 2.2 gives,

$$G_{Rad} + G_{Diff} = G_{Therm} = \frac{\partial P_{DS}}{\partial T_D} \quad 3.8$$

In Equation 3.8, G_{Therm} defines the total thermal conductance of the detector, provided by the parallel thermal radiation and thermal diffusion processes.

The NEP due to diffusion gives the thermal diffusion noise in a TTD,

$$< NEP_{Diff} >^2 = 4kT^2BG_{Diff}, \quad 3.9$$

Where, G_{Diff}, is the thermal diffusion conductance of the detector. The total thermal noise power is given by the sum of the thermal radiation noise and the thermal diffusion noise,

$$< NEP_{Therm} >^2 = 4kT^2BG_{Therm}, \quad 3.10$$

In terms of noise currents, the thermal noise is given by,

$$< i_{Therm}^2 >= \frac{4kT^2}{C_{Therm}}\left(\frac{\partial I}{\partial T}\right)^2, \quad 3.11$$

where C_{Therm} is the thermal capacitance of the pixel.
In zero bias steady state, Equation 3.4 can be rewritten as,

$$\frac{A_{Eff}\varepsilon_D\sigma T_S^4}{4F^2+1}+\left(1-\frac{1}{4F^2+1}\right)A_{Eff}\varepsilon_D\sigma T_B^4-A_{Eff}\varepsilon_D\sigma T_D^4-G_{Diff}(T_D-T_B)=0 \qquad 3.12$$

Expanding in a Taylor series about T_B,

$$\frac{4A_{Eff}\varepsilon_D\sigma T_B^3(\Delta T_S)}{4F^2+1}+4\left(1-\frac{1}{4F^2+1}\right)A_{Eff}\varepsilon_D\sigma T_B^3(0)-4A_{Eff}\varepsilon_D\sigma T_B^3(\Delta T_D)-G_{Diff}\Delta T_D=0 \qquad 3.13$$

or,

$$\frac{G_{Rad}\Delta T_S}{4F^2+1}-G_{Rad}\Delta T_D-G_{Diff}\Delta T_D=0. \qquad 3.14$$

Equation 2.2 can be substituted into Equation 3.14 to determine the temperature transfer gain between the observed scene and the detector element $\Delta T_D/\Delta T_S$.

$$\frac{\Delta T_D}{\Delta T_S}=\frac{1}{4F^2+1}\left(\frac{G_{Rad}}{G_{Rad}+G_{Diff}}\right) \qquad 3.15$$

The thermal diffusion isolation of a pixel can only be ignored if the radiative heat loss from the pixel is much larger than the diffusive heat loss from the pixel, that is:

$$G_{Rad} >> G_{Diff} \qquad 3.16$$

Under that condition, the sensor becomes background radiation limited and the sensor temperature transfer gain becomes:

$$\frac{\Delta T_D}{\Delta T_S}=\frac{1}{4F^2+1}. \qquad 3.17$$

Most current day thermal sensors are thermal diffusion limited and relationships 3.16 and 3.17 do not apply.

The thermal response time of the thermionic thermal detector pixel is given by,

$$\tau=\frac{C_{Therm}}{G_{Therm}} \qquad 3.18$$

where C_{Therm} is given by

$$C_{Therm}=A_D\rho c_s t_f. \qquad 3.19$$

where t_f is the SOI silicon film thickness.

4. ELECTRICAL EQUATIONS

The current density in a Schottky diode based thermal detector is calculated from thermionic emission theory,[7]

$$J = J_S(e^{qV/kT} - 1), \qquad 4.1$$

where kT is the thermal energy and J_S the saturation current density.

When the detector is operated under back bias, at voltages large compared to kT/q, the reverse current density J_R reduces to the saturation current density.

$$J_R = J_S = A^{**}T^2 e^{-q\Phi_{bn}/kT} \qquad 4.2$$

Where, $q\phi_{bn}$ is the Schottky barrier potential at the operating bias V and A^{**} is the modified Richardson constant. The barrier potential at the operating bias is reduced from the zero bias Schottky potential by image lowering, to a level given by:

$$\Phi_{bn} = \Phi_{bo} - \sqrt{\frac{qE}{4\pi\varepsilon_{si}}} \qquad 4.3$$

Where $q\phi_{bo}$ is the Schottky barrier potential at zero bias, E is the electric field and ε_{si} is the dielectric constant of silicon. The peak electric field for an impurity concentration, N, is given by:

$$E = \sqrt{\frac{2qN}{\varepsilon_{si}}(V_{bi} - V - kT/q)} \qquad 4.4$$

where qV_{bi} is the diode built in potential. We can exploit image lowering to adjust the Schottky barrier potential, so as to optimize the detector operating current.

Neglecting the small temperature dependence of the electric field in Equation 4.4, the change in the reverse current in a thermionic detector as a function of temperature, $\partial J_R/\partial T$, is given by:

$$\frac{\partial J_R}{\partial T} = T\left(\frac{q\Phi_{bn}}{kT} + 2\right)A^{**}e^{-q\Phi_{bn}/kT} \qquad 4.5$$

The resulting TTD temperature coefficient, $(1/J_R)\partial J_R/\partial T$, is given by:

$$\frac{1}{J_R}\frac{\partial J_R}{\partial T} = \frac{1}{T}\left(\frac{q\Phi_{bn}}{kT} + 2\right). \qquad 4.6$$

For a TTD with a 0.36 eV Schottky potential, the temperature coefficient, $(1/J_R)\partial J_R/\partial T$, is **6%/K** at room temperature.

The shot noise in a TTD is given by,

$$< i_{Shot}^2 >= 2qBI_R = 2qBA_{Eff}J_R \qquad 4.7$$

Where B is the measurement bandwidth and I_R is the reverse bias diode current.[8]
Thus,

$$< i_{Shot}^2 >= 2qBA_{Eff}\,A^{**}T^2 e^{\frac{-q\phi_{bn}}{kT}}. \qquad 4.9$$

The Johnson noise in a TTD is given by,

$$< i^2_{Johnson} >= \frac{4kTB}{R_{det}}, \quad 4.10$$

where R_{det}, is the differential diode resistance, which can be written as,

$$\frac{1}{R_{det}} = A_{Eff}\frac{\partial J}{\partial V} = \frac{qA_{Eff}}{kT} J_S e^{qV/kT}, \quad 4.11$$

and the large signal resistance can be written as,

$$R_{Det} = \frac{V}{A_{Eff}J_S} = \frac{V}{A_{Eff}J_S(e^{qV/kT}-1)} \approx \frac{V}{A_{Eff}J_S}. \quad 4.12$$

The Johnson noise resistance in Equation 4.10 is a small signal parameter, given by Equation 4.11; consequently,

$$< i^2_{Johnson} >= 4qBAJ_S e^{qV/kT}. \quad 4.13$$

The TTD is operated under modest reverse bias, which is large compared to kT/q, so Johnson noise is generally negligible.

In the absence of 1/f-noise, the total electrical noise becomes:

$$< i^2_{Electrical} >=< i^2_{Johnson} > + < i^2_{Shot} >, \quad 4.14$$

which can be expressed as:[9]

$$< i^2_{Electrical} >= 2qBJ_R A_{Eff}\left(e^{qV/kT}+1\right) \quad 4.15$$

5. MULTIPLEXER AND AMPLIFIER

Fig. 2 describes an architecture similar to the one used in standard, VO_x based, microbolometer arrays. Each pixel is composed of a thermally sensitive Schottky diode and a row selection transistor. The row select turns on all unit cell transistors in a row, to simultaneously bias a detector element in each column. The reverse bias potential of the Schottky diode is determined by the difference between the reference voltage at the diode semiconductor electrode and the bias potential at the diode metal contact. The metal contact potential is set at each column bus. At the bottom of each column in the array are two transimpedance amplifiers, a differential amplifier, a column select transistor and a reference pixel, which is shielded from incident radiation. The current in the reference pixel is clamped to the substrate temperature T_b. Applying the bias potential to the positive input of the transimpedance amplifier sets the column bus potential. A similar bias potential is applied to the column of the reference pixel for bias current subtraction at the differential amplifier. The transimpedance amplifier converts the detector current to a voltage. The differential amplifier provides differential suppression of DC bias, and a programmable integration time. This amplifier is also used to dynamically correct for pixel to pixel nonuniformity.
The dynamic range of the output and the pixel to pixel nonuniformity of the signal from the array limits the gain of the amplifier. As the uniformity of the signal from each of the pixels in the array is improved, a higher gain differential amplifier can be used without clipping the signal. Improved uniformity will also allow equal sensitivity with a reduced dynamic range A/D converter, resulting in lower sensor cost.

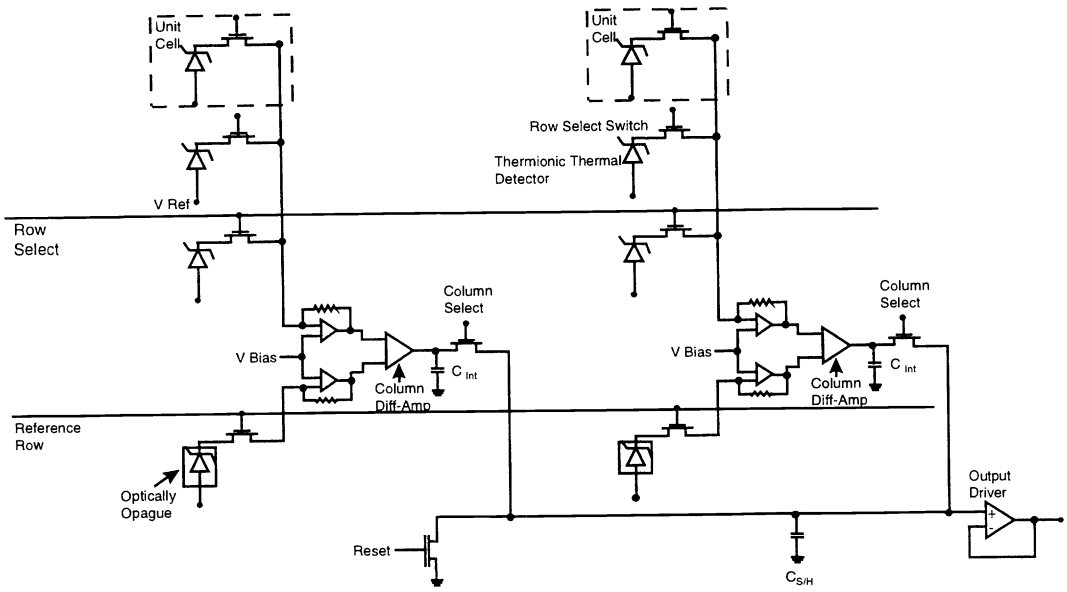

Figure 2: Schematic view of TTD based thermal imaging array

The input current noise of the amplifier, i_{na}, is given by the input referred voltage noise divided by the load resistance to the amplifier, namely,

$$i_{na} = \frac{v_{na}}{R_L} = \frac{v_{na}(R_{det} + R_F)}{R_{det} R_F}, \qquad 5.1$$

with the load resistance given by the parallel combination of the detector resistance and the feedback resistance. Consequently,

$$i^2_{Amp} = 2\frac{v^2_{na}}{R^2_L} = 2v^2_{na}\frac{(R_{det} + R_F)^2}{(R_{det} R_F)^2} \qquad 5.2$$

The factor of two arises from the noise of two transimpedance amplifiers in the output multiplexer adding in quadrature. Using the small signal resistance of the TTD as the detector resistance,

$$i^2_{Amp} = 2v^2_{na}\left(1/R_F + \frac{qA_{Eff}}{kT} J_S e^{qV/kT}\right)^2. \qquad 5.3$$

R_F is selected to be large, approximately 1 MΩ, to minimize the contribution of multiplexer noise to the total noise.

6. NOISE EQUIVALENT TEMPERATURE

The total noise in the TTD is given by the quadrature sum of all the contributing noise sources, namely,

$$< i^2_{Tot} >=< i^2_{Johnson} > + < i^2_{Shot} > + < i^2_{Thermal} > + < i^2_{amplifier} >. \qquad 6.1$$

where the thermal noise is the sum of the thermal noise due to radiation and the thermal noise due to diffusion. Substituting for each of these terms, and noting Equation 4.15 we find:

$$< i_{Tot}^2 >= 2qBA_{Eff}J_S\left(e^{qV/kT_D}+1\right)+\frac{4kT_D^2}{C_{Therm}}\left(\frac{A_{Eff}\partial J_S}{\partial T_D}\right)^2+2v_{na}^2\left(\frac{1}{R_F}+\frac{qA_{Eff}}{kT_D}J_S e^{qV/kT_D}\right)^2 \quad 6.2$$

or,

$$< i_{Tot}^2 >= 2qBA_{Eff}J_S\left(e^{qV/kT_D}+1\right)+\frac{4kT_d^2}{C_{Therm}}\left(\frac{A_{Eff}J_S}{T_D}\left[\frac{q\Phi_{bo}}{kT_D}-\frac{q\sqrt{qE/4\pi\varepsilon_{si}}}{kT_D}+2\right]\right)^2 \quad 6.3$$
$$+2v_{na}^2\left(\frac{1}{R_F}+\frac{qA_{Eff}}{kT_D}J_S e^{qV/kT_D}\right)^2$$

Equation 6.3 is accurate in the absence of any simplifying approximations describing the magnitude of the applied bias or the relative values of these noise terms. Equation 6.3 is the noise term in the model used to generate the theoretical performance graphs in this paper.

At any significant reverse bias above kT/q (V_{Rev} > 100mV), and with a reduced barrier potential Φ_{bn}, the diode current can be assumed to be the saturation current. In addition, the diode impedance becomes very large, so as to give a negligible contribution to the amplifier noise. Under these conditions Equation 6.3 becomes:

$$< i_{Tot}^2 >= 2qBA_{Eff}J_S+\frac{4kT_D^2}{C_{Therm}}\frac{A_{Eff}^2J_S^2}{T_D{}^2}\left(\frac{q\Phi_{bn}}{kT_D}+2\right)^2+2\frac{v_{na}^2}{R_F^2} \quad 6.4$$

$$< i_{Tot}^2 >= 2qBA_{Eff}J_S+\frac{4kA_{Eff}^2J_S^2}{C_{Therm}}\left(\frac{q\Phi_{bn}}{kT_D}+2\right)^2+2\frac{v_{na}^2}{R_F^2} \quad 6.4a$$

For small temperature differences, the NEΔT in a Thermionic Thermal Detector is given by:

$$NE\Delta T=\frac{(T_S-T_B)\sqrt{< i_{Tot}^2 >}}{A_{Eff}J_S(T_D)-A_{Eff}J_S(T_B)}, \quad 6.5$$

where $J_S(T_B)$ is the saturation current of a diode that is imaging the background and $J_S(T_D)$ is the saturation current of the diode that is imaging the target. The diode shot noise current is given by the first term in Equation 6.4. If the dominant noise in the system is the diode shot noise and (T_S-T_B) = 1 K, Equation 6.5 becomes:

$$NE\Delta T=\frac{\sqrt{2qBA_{Eff}J_S(T_D)}}{A_{Eff}J_S(T_D)-A_{Eff}J_S(T_B)}. \quad 6.6$$

7. PERFORMANCE CALCULATIONS OF THE THERMIONIC THERMAL DETECTOR AT 200K, 300K, AND 400K

The graphs in Fig. 3 illustrate the performance of a TTD sensor, as described by the above model. The top curve represents the performance of the TTD as a function of the pixel fill factor, using a typical pixel size with a thermal conductance of $5x10^{-8}$ W/K. At a modest 70% fill factor (for a hybrid array), the NEDT of the TTD is predicted to be 6 mK. The bottom curve illustrates the theoretical best performance of the TTD with a thermal isolation conductance of 10^{-8}

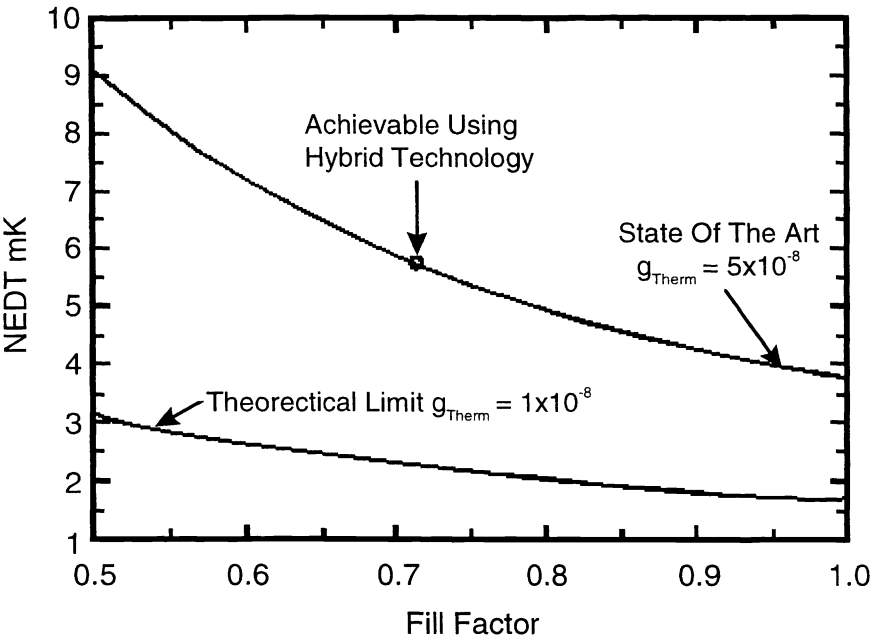

Figure 3: NEDT performance of a TTD 320x244 array with a 50x50 μm^2 pixel size, 0.36 eV barrier height, operating in the 8-14 μm band with F/1 optics.

Fig. 4 shows a representative Richardson activation energy plot of a Schottky barrier diode at different reverse biases. This device was fabricated at the Air Force Research Laboratory. The substrate was a SIMOX p-type 10-20 ohm-cm wafer with 5.16 μm of surface silicon. Further processing was done to define the active area and create an ohmic contact. 10 nm of a metal was deposited to form the silicide. The activation energy is obtained by measuring the dark current as a function of temperature. A variety of different metals and process flows have been used to fabricate devices with barrier heights ranging from 0.22 eV to 0.48 eV. Notice that in a single diode, an approximately 1 volt change in bias can change the bias current two orders of magnitude. This will support sensor optimization over temperature ranges of tens of degrees K.

In a separate experiment a PtSi photoemissive array was operated at 80 K. The array was compensated, when focused on a blank wall; so as to have a flat image. Then, the temperature was allowed to rise, so that thermionic dark current dominated the signal. The dark current slowly degraded the sensor noise by the addition of both thermionic emission shot noise and pattern noise. The temperature was increased by more than 6K, before the noise doubled. Thus, a TTD sensor should be capable of operating over ambient temperature ranges greater than 50C, without recalibration.

In the following analysis, we consider the model for NEDT given by Equation 6.5 at three operating temperatures, 200K, 300K, and 400K. These temperatures correspond to different operating environments, namely, space using passive cooling, room temperature uncooled with thermoelectric stabilization, and high temperature with heat stabilization. The theoretical performance demonstrated by Figs. 5, 6, 7 are for a 320x244 array with a 50x50 μm^2 pixel size, $5x10^{-8}$ W/K thermal conductivity, operating in the 8-14 μm band using F/1 optics, at various fill factors. The sample current is typically limited to approximately 150 μA by the power handling capability of the multiplexer, corresponding to a sample charge of approximately 10 billion electrons.

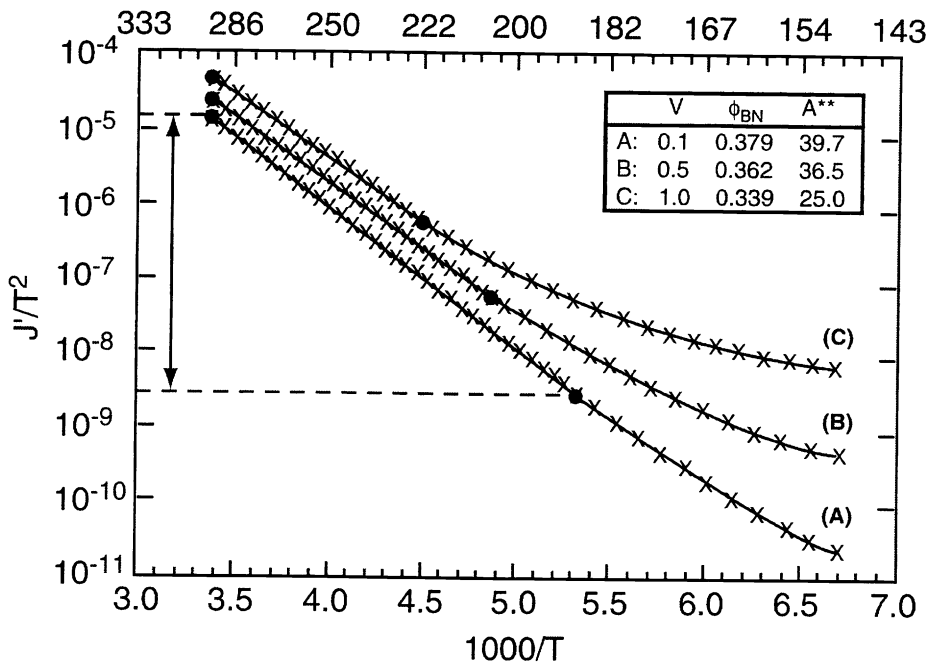

Figure 4: Richardson activation energy curves for a 0.36 eV Schottky diode fabricated on SOI, with applied reverse bias voltages, 0.1 V, 0.5 V, and 1.0 V. The Schottky barrier potential Φ_{bn} and Richardson constant A^{**} are determined by fitting these curves. The observed characteristics are typical of high quality metal-silicide / silicon devices.

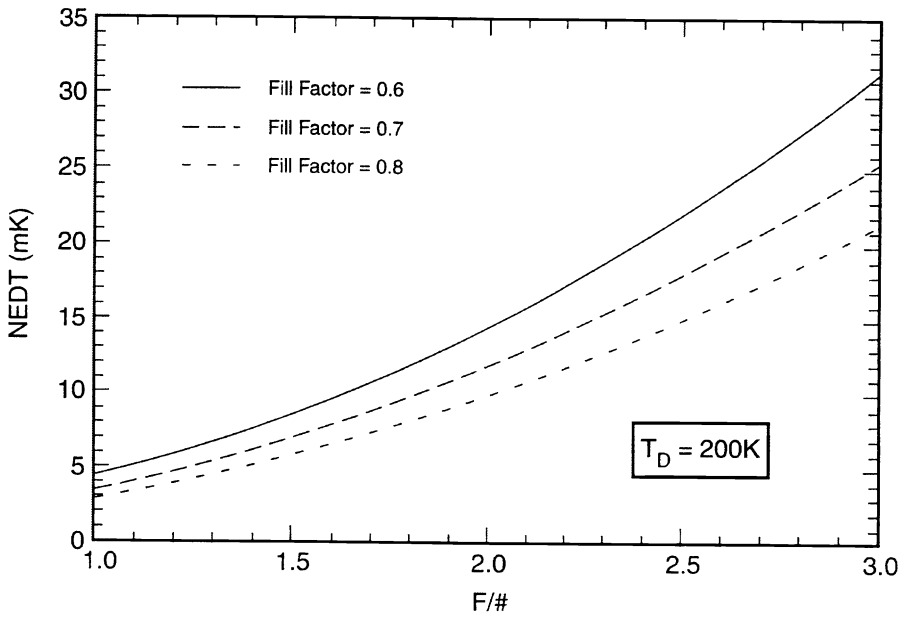

Figure 5: NEDT performance of a TTD sensor at 200K, based on a 320x244 array with a 50x50 μm^2 pixel size, 0.23 eV barrier potential, $5x10^{-8}$ W/K thermal conductance operating in the 8-14 μm band.

Fig. 5 shows the operation of the TTD at 200K with a 0.23 eV barrier. The graph is of the noise equivalent temperature as a function of f/#. It does not consider the effect of cavity cooling thus the graph understates expected performance. The NEDT of the TTD is predicted to be 4 mK at f/1. The temperature coefficient is 7 %/K, total noise current is 4.19×10^{-19}amperes and the signal to noise ratio is 1.6×10^4. The doping concentration in the Si film is $3 \times 10^{15} cm^{-3}$. This device will be capable of operating in a space environment using passive cooling techniques.

Fig. 6: shows the TTD operating at room temperature, 300K, using a 0.36 eV barrier. At 300K, the NEDT increases to 6 mK and the temperature coefficient is 6%/K. The total noise current is 4.13×10^{-19}amperes and the signal to noise ratio is 1.1×10^4. The doping concentration in the Si film is $2 \times 10^{15} cm^{-3}$. The uncooled performance of the TTD is competitive with a VO_x based microbolometer, and can be used in the same applications, such as maintenance free remote sensing, surveillance and night vision. The TTD diode sensing element can produce the required 150 μA of sample current using substantially lower voltage than that required by a VO_x resistor. Consequently, temperature stabilization of a TTD array can be achieved by thermoelectric techniques using substantially less power. For example, consider two devices operating at 300K, the biasing required for the microbolometer is greater than 2 V while the biasing required for the diode is 4KT, or approximately 100 mV. Assuming the VO_x is biased to 2 V and the diode biasing is 0.5 V, the power required for a 320x244 VO_x microbolometer is 325 μW compared to 75 μW for a TTD array.

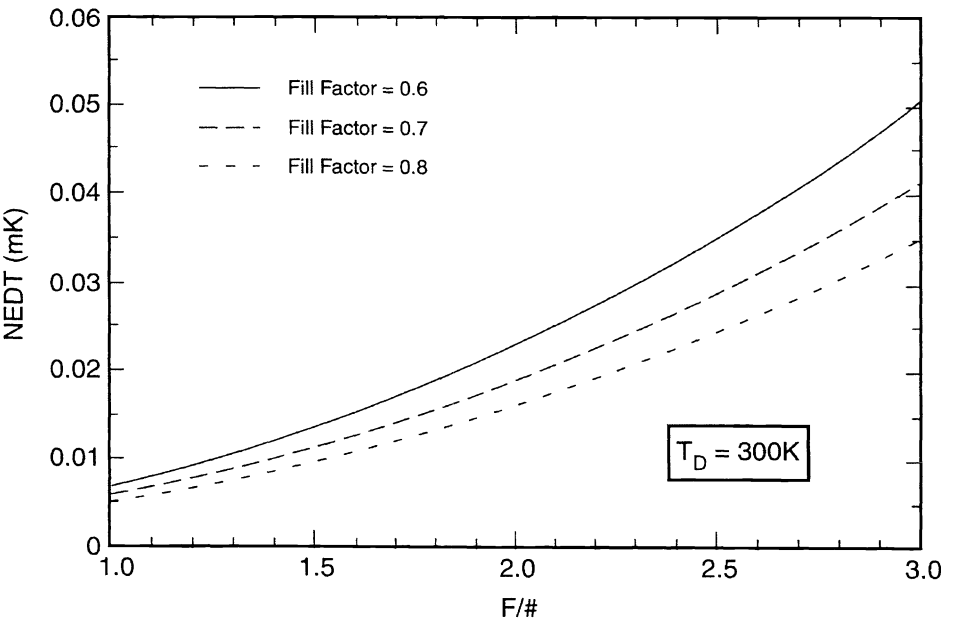

Figure 6: Uncooled NEDT performance of a TTD sensor at 300K, based on a 320x244 array with a 50x50 μm^2 pixel size, 0.36 eV barrier potential, 5×10^{-8} W/K thermal conductance operating in the 8-14 μm band.

Fig. 7 illustrates the performance of the TTD at 400K using a 0.45 eV barrier. The NEDT has increased to 10 mK and the temperature coefficient has decreased to 4%/K. The total noise current is 4.24×10^{-19}amperes and the signal to noise ratio is 8.9×10^3. The doping concentration in the Si film is $5 \times 10^{15} cm^{-3}$. Since temperature stabilization by heating is 10-100 times more efficient than temperature stabilization by cooling, military applications with high temperature operating environments may see significant additional power savings.

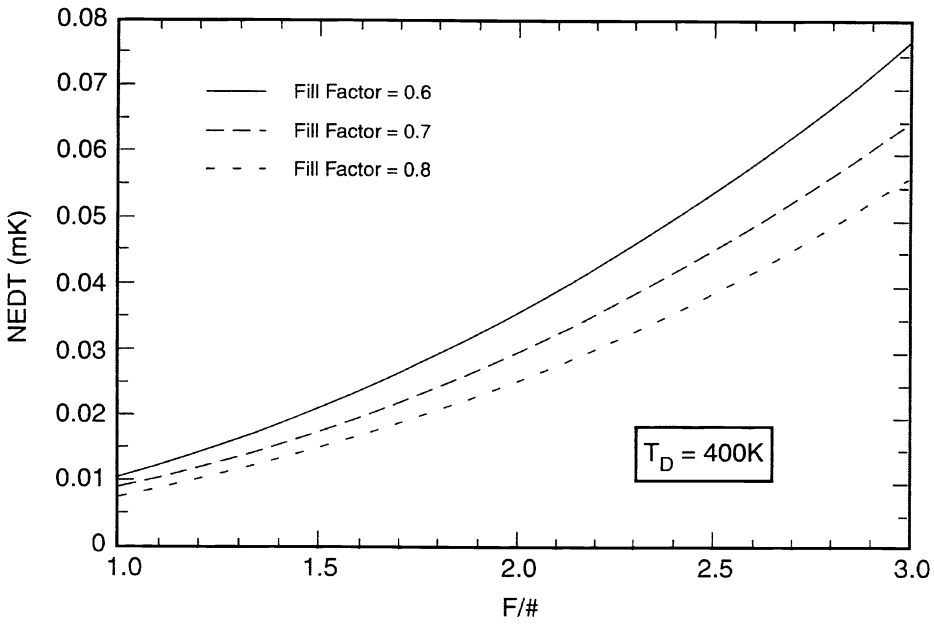

Figure 7: NEDT performance of a TTD sensor, at 400K, based 320x244 array with a 50x50 μm^2 pixel size, 0.45 eV barrier height, $5x10^{-8}$ W/K thermal conductance operating in the 8-14 μm band.

Fig. 8 Gives the variation of NEDT and temperature coefficient (dI/dT)/I, based on Equation 4.6 for (dI/dT)/I and Equation 6.5 for NEDT. At constant current of 150 μA, NEDT increases and (dI/dT)/I decreases with temperature. The increase in (dI/dT)/I is approximately 0.025 $\%/K^2$ and the decrease in NEDT is approximately 0.015 mK/K.

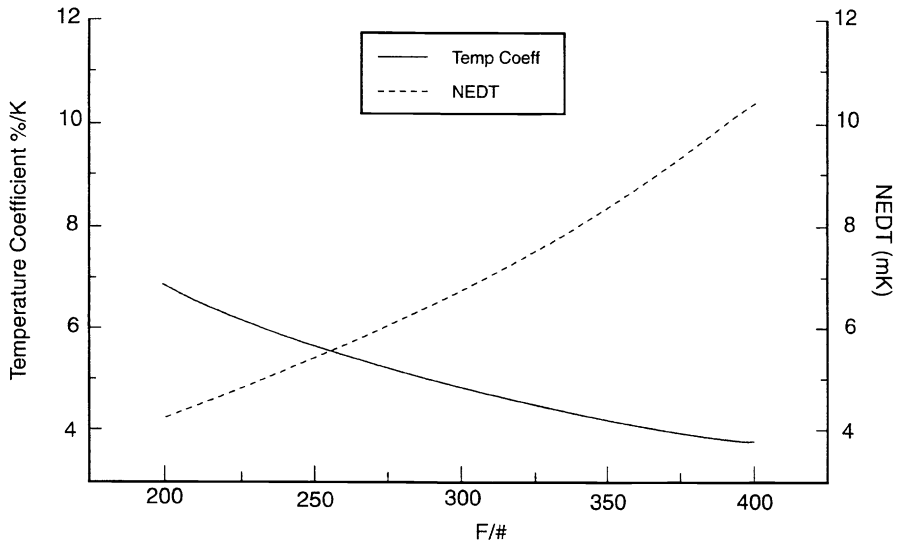

Figure 8: Temperature coefficient and NEDT of various barrier heights and doping levels as a function of operating temperature.

8. CONCLUSION

We have described the application of thermionic emission in metal-silicide/silicon Schottky barrier diodes to thermal detection and imaging. We refer to these devices as thermionic thermal detectors or TTDs. TTDs offer several advantages relative to current microbolometer devices. TTDs are fabricated using standard silicon microcircuit processing technology. TTDs are not restricted to operate at a particular temperature. In fact, by selection of a particular metal-silicide, substrate doping and operating voltage, TTD sensors can be designed to operate over a 200C temperature span. Over this wide temperature range, individual sensors would be based on a common multiplexer design. Individual detector designs can be biased to have optimum sensitivity over tens of degrees C (see Figure 4).

Metal-silicide thermionic emission arrays have the same noise characteristics as PtSi MWIR photoemission arrays, including absence of 1/f-noise, shot noise dominance and exceptional cell to cell uniformity.

At 300K the TTD thermal coefficient (dI/dT)/I is 6%/K, a threefold advantage over current art devices. The use of a diode as a sensing element results in at least a five-fold reduction in power dissipation during detector sampling. Using a current art multiplexer with a 5x10-8 W/K thermal conductance, these characteristics will support an f/1 uncooled thermal imager, with 50mm2 detectors, having a 6 mK NEDT. The same technology supports NEDTs ranging from 4 mK to 10 mK, over a temperature range from 200K to 400K.

At ambient temperature, the use of thermionic emission based TTDs in uncooled thermal imaging offers advantages of improved performance, simpler fabrication and potential cost reduction. At 200K the technology provides the basis for passively cooled LWIR imaging from space. Between 300K and 400K the technology will support thermal imaging sensors for high performance missiles. These sensors can be designed to be tolerant of transient heating of the missile dome, during flight. Simple, low cost, heating circuits can be used to control the focal plane substrate temperature.

REFERENCES

[1] Electronics: Microstructure Science, edited by N. Einspruch, "Formation and Characterization of Transition Metal Silicides," M. Nicolet and S. Lau, Academic Press, 1983, NY.

[2] T. G. Stratton, B. E. Cole, P. W. Kruse, R. A. Wood, et al., "High Temperature Superconducting Microbolometer," App. Phys. Lett. 57(1), July 1990.

[3] R. A. Wood, et al., "Uncooled Thermal Imaging with Monolithic Silicon Focal Plane Arrays," Proc. SPIE 2020, Infrared Technology XIX, 329, 1993.

[4] B. R. Johnson, P. W. Kruse, "Silicon Microstructure Superconducting Microbolometer Infrared Arrays," Proc. SPIE 2020, Infrared Technology XIX, 2-11, 1993.

[5] J. Choi, Y. Park and H. Min, "Extremely Thin SOI MOSFET Characteristics Including Inversion Layer to Accumulation Layer Tunneling" IEDM, 27.1.1, 1994.

[6] R. J. Keyes, Optical and Infrared Detectors, Chapter 3, pp. 74, Springer Verlag, 1980.

[7] S. M. Sze, Physics of Semiconductor Devices, Chapter 5, John Wiley & Sons, 1981.

[8] S. M. Sze, Ibid. pp. 111-112.

[9] S. M. Sze, Ibid. pp. 130-131.